

Threshold voltage control of Pt-Ti-O gate Si-metal-insulator semiconductor field-effect transistors hydrogen gas sensors by using oxygen invasion into Ti layers

Toshiyuki Usagawa and Yota Kikuchi

Citation: [Journal of Applied Physics](#) **110**, 074515 (2011); doi: 10.1063/1.3645028

View online: <http://dx.doi.org/10.1063/1.3645028>

View Table of Contents: <http://scitation.aip.org/content/aip/journal/jap/110/7?ver=pdfcov>

Published by the [AIP Publishing](#)

Articles you may be interested in

[Control of normally on/off characteristics in hydrogenated diamond metal-insulator-semiconductor field-effect transistors](#)

J. Appl. Phys. **118**, 115704 (2015); 10.1063/1.4930294

[Suspended core-shell Pt-PtOx nanostructure for ultrasensitive hydrogen gas sensor](#)

J. Appl. Phys. **117**, 224501 (2015); 10.1063/1.4922240

[A Pt-Ti-O gate Si-metal-insulator-semiconductor field-effect transistor hydrogen gas sensor](#)


J. Appl. Phys. **108**, 074909 (2010); 10.1063/1.3483942

[Characterization of bulk GaN rectifiers for hydrogen gas sensing](#)

J. Vac. Sci. Technol. B **23**, 2373 (2005); 10.1116/1.2110343

[Ti gate compatible with atomic-layer-deposited HfO₂ for n-type metal-oxide-semiconductor devices](#)

Appl. Phys. Lett. **86**, 092107 (2005); 10.1063/1.1871362




SHIMADZU
Excellence in Science

Powerful, Multi-functional UV-Vis-NIR and FTIR Spectrophotometers

Providing the utmost in sensitivity, accuracy and resolution for applications in materials characterization and nano research

- Photovoltaics
- Polymers
- Thin films
- Paints
- Ceramics
- DNA film structures
- Coatings
- Packaging materials



[Click here to learn more](#)

Threshold voltage control of Pt-Ti-O gate Si-metal-insulator semiconductor field-effect transistors hydrogen gas sensors by using oxygen invasion into Ti layers

Toshiyuki Usagawa^{a)} and Yota Kikuchi

Central Research Laboratory, Hitachi, Ltd., Kokubunji, Tokyo 185-8601, Japan

(Received 12 May 2011; accepted 25 August 2011; published online 13 October 2011)

Although the threshold voltages (V_{th}) of the as-processed Pt(15 nm)/Ti(5 nm)-gate Si-MOSFETs under same channel ion dose conditions show a large variation such as 0.846 V among several wafers, the air-annealing and succeeding hydrogen post-annealing procedure for the FETs hydrogen gas sensors leads to excellent uniform V_{th} distributions and large sensing amplitude ΔV_g . The oxygen invasion process through Pt grain boundaries to amorphous Ti layers at 400 °C air-annealing for two hours is not a simple dopant diffusion process but super-heavily oxygen-doped process partly to grow nano-crystalline TiOx. The oxygen-invaded Ti layers change to a kind of new materials; novel mixing layers of nano-crystalline TiOx and super-heavily oxygen-doped amorphous Ti formed on SiO₂/Si substrates. The Ti mixing layers change from metals to semiconductors or insulators. As the Ti layers are so thin like 5 nm, the total amount of oxygen invaded into Ti layers will be saturated and stabilized. From the device operation point of view, it is crucial to control the V_{th} precisely that the Ti novel mixing layers are thin and fully depleted. This is supported by the fact that the V_{th} change before and after air-annealing procedures can be well explained by the difference of vacuum work function between Pt and Ti. © 2011 American Institute of Physics. [doi:10.1063/1.3645028]

I. INTRODUCTION

Recently much attention has been paid to hydrogen gas sensors because renewable energy systems, such as solar or hydrogen energy, require reliable hydrogen safety monitoring sensor systems that can withstand harsh open-air environments. As one of the possible candidates for such applications, we have proposed a novel platinum-titanium-oxygen (Pt-Ti-O)-gate Si-metal-insulator semiconductor field-effect transistors (MISFETs) hydrogen gas sensor.¹⁻³ The Pt-Ti-O gate Si-MISFETs hydrogen gas sensors are typically fabricated by annealing Pt(15 nm)/Ti(5 nm)-gate Si-MOSFETs in air at 400 °C for two hours. Our sensors consist of unique gate structures composed of Ti and oxygen accumulated regions around Pt grains on top of a novel mixing layer of nanocrystalline TiOx and superheavily oxygen-doped amorphous Ti formed on SiO₂/Si substrates. The Pt-Ti-O gate Si-MISFETs hydrogen gas sensors after hydrogen annealing procedure show excellent sensor characteristics, in which the sensing amplitude ΔV_g , defined by the magnitude of threshold voltage V_{th} shifts under the hydrogen exposure, can be well fitted by a linear function of the logarithm of hydrogen concentration C (ppm) between 100 ppm and 1% of air-diluted H₂ concentrations,

$$\Delta V_g(V) = 0.355 \log C(\text{ppm}) - 0.610, \quad (1)$$

where $\log C(\text{ppm})$ denotes the common logarithm of $C(\text{ppm})$.² As the standard definition of the sensitivity derived from the derivative of $\Delta V_g(V)$ versus $C(\text{ppm})$ leads to con-

centration dependent sensitivity, we have introduced alternative constant sensitivity per decade. In our papers, the gradient 0.355 V represents the sensitivity of the fabricated FET sensors, which is about ten-times larger than the value of 35.5 mV/decade at 115 °C compared with hitherto developed Pt-gate Si-MOSFETs hydrogen gas sensors or the expected value of 38.5 mV/decade from Nernst equation.⁴ The sensing range seems to be suitable for most hydrogen safety monitoring sensor systems. Furthermore the long intrinsic lifetime more than 10 years has been reported from preliminary accelerated temperature and/or humidity aging tests about the Pt-Ti-O gate Si-MISFETs hydrogen gas sensor chips.^{3,5} The Pt-Ti-O gate structures are determined with the help of transmission electron microscope (TEM), X-ray diffraction, Auger analysis, and TEM energy dispersive X-ray spectroscopy (EDX) analysis before and after air annealing.¹⁻³

One of the most novel features about device operations of Pt-Ti-O gate Si-MISFETs hydrogen gas sensors is a way of controlling the threshold voltage V_{th} by using oxygen invasion into titanium layers from open air through thin platinum layers. It shows us a serious question about the controllability of V_{th} because precise control of V_{th} of Si-MOSFETs will be impossible even if by using the most prevailed dopant diffusion process by gaseous sources such as AsH₃ instead of ion implantation⁶ and/or the annealing temperature of 400 °C is too low as the oxidation temperature of Ti layers. In fact, some of the preliminary experimental results showed that threshold voltages of as processed Pt(15 nm)/Ti(5 nm)-gate Si-MOSFETs were scattered among wafers under the same dose conditions of ion implantation. Sensing amplitudes were scattered so much over the wafers including the samples without any hydrogen responses.^{2,7}

^{a)}Author to whom correspondence should be addressed. Electronic mail: toshiya.usagawa.gv@hitachi.com. FAX: +81-42-327-7722.

TABLE II. List of ion dose conditions.

Dose conditions	(A)	(B)	(C)	Implantation Energy
Chip no.	#2, #3	Others	#8	
n-type FET (cm^{-2})	0.8×10^{12}	1.0×10^{12}	1.2×10^{12}	P^+ 80 keV
p-well (cm^{-2})		7.6×10^{12}		BF_2^+ 60 keV
p-type FET (cm^{-2})	3.2×10^{12}	4.0×10^{12}	4.8×10^{12}	BF_2^+ 80 keV
n-well (cm^{-2})		1.15×10^{13}		P^+ 125 keV
Si substrate (cm^{-3})		8.0×10^{14} (p-type)		

and finally changes to pure air gas. The flow rate of the hydrogen gas and air gas is 0.5 L/min. The standard H_2 concentration is 1000 ppm for device characterizations. To reduce power consumption, we selected enhancement-type FETs so that most of the operation range of the gate voltage V_g covers the saturated regions of the pentode I-V characteristics for the fabricated Si-MOSFETs at $V_{ds} = 1.5$ V, where the source-drain currents are nearly independent of the source-drain voltage at around 1.5 V. We have used the tentative V_{th} defined by the gate voltage V_g for $I_{ds} = 10 \mu\text{A}$ at a source-drain voltage $V_{ds} = 1.5$ V with short-circuiting source and p-well for n-type FETs. These measuring conditions are applied to evaluate ΔV_g , unless otherwise specified.

III. DEVICE CHARACTERISTICS

A. Pt-Ti-O gate Si-MISFETs hydrogen gas sensors

In our previous papers,^{1,2} we reported a significant increase in ΔV_g by annealing sensor chips composed of Pt(15 nm)/Ti(5 nm)-gate Si-MOSFETs in air at 400 °C for two hours. In this section we have investigated optimum air-annealing conditions for Pt(15 nm)/Ti(5 nm)-gate Si-MOSFETs by changing annealing temperature and time. The experimental results in the Appendix show that the previous air-annealing conditions at 400 °C and two hours were nearly optimum to realize Pt-Ti-O gate Si-MISFETs hydrogen gas sensors.² Therefore, we have fixed tentatively the standard annealing temperature and time to 400 °C and two hours with little bit larger margins. Hereafter, this procedure is referred to as “air annealing”.

Although the ΔV_g of #2U, #3U, #8U, #23U, and #24U chips show extremely high values between 0.821 ~ 0.958 V after air annealing, there remains rather high residual sensing amplitudes ΔV_{gres} (as annealed) to show slow damping tails in common.^{1,2} As was discussed in our previous paper,² we found a stable response with reduced ΔV_{gres} , 0.05 V, after 10 min of air-diluted 1000-ppm hydrogen exposure at 115 °C for the air-annealed samples. Hereafter, this procedure was referred to as “hydrogen post-annealing”. The hydrogen post-annealing procedure decreases V_{th} by nearly the same value of ΔV_{gres} (as annealed) in terms of terminating the deep traps generated around the gate insulator surface during air annealing. As a typical example, the response curves of ΔV_g for #24C before and after air annealing, and also after hydrogen post-annealing, are shown in Fig. 3. The sensing amplitudes of ΔV_g for the hydrogen post-annealed Pt-Ti-O

gate Si-MISFETs hydrogen gas sensors are well described by Eq. (1).

B. Oxygen invasion process for Pt(15 nm)/Ti(5 nm)-gate Si-MOSFETs

Our main concerns are to clarify the correlation among oxygen invasion process, V_{th} changes and sensor characteristics. In our tuning of V_{th} , phosphorus ions are implanted into the p-well. By considering channel ion implantation using P^+ with an implantation energy of 80 keV depending on the wafer for three different doses of Table II: (A) $0.8 \times 10^{12} \text{ cm}^{-2}$, (B) $1.0 \times 10^{12} \text{ cm}^{-2}$, and (C) $1.2 \times 10^{12} \text{ cm}^{-2}$ for n-type FETs, the difference between adjacent two doses, N_{DS} , is $2.0 \times 10^{11} \text{ cm}^{-2}$. In our doping conditions of the channel and the p-well, the depletion layer of the PN junction extends to the gate oxide SiO_2/Si interface, and the corresponding V_{th} shift, ΔV_{th} , between adjacent two doses is given by the following equation,⁸

$$\Delta V_{th} = qN_{DS}/C_{OX}, \quad (2)$$

where q is the unit charge and C_{OX} is the gate capacitance per unit area. By using the relative dielectric constant and the thickness of gate silicon dioxide SiO_2 as 3.9 and 18 nm, Equation (2) leads to $\Delta V_{th} = 0.167$ V.

Figures 4(a) and 4(b) show the accumulated data of wafer distributions of V_{th} and ΔV_g for several as processed Pt(15 nm)/Ti(5 nm)-gate Si-MOSFETs sensor chips, as processed Pt(90 nm)/Ti(5 nm)-gate #E-1 chips, and hydrogen post-annealed #A-2 chips after air-annealing at 400 °C for 8 h in Table I. The sensor chips are classified by three different doses of Table II. The sample #4 ref denotes the

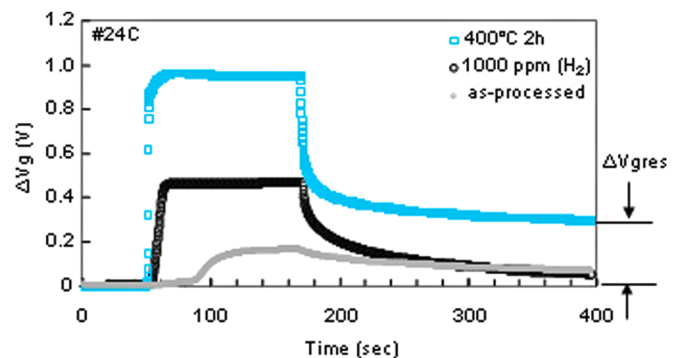


FIG. 3. (Color online) Response curves of ΔV_g for #24C sensor FETs: as-processed chip, air-annealed chip after 400 °C 2-h annealing in air, and hydrogen post-annealing chip (exposed to 10 min of air-diluted 1000-ppm H_2 at 115 °C after 400 °C 2-h annealing in air).

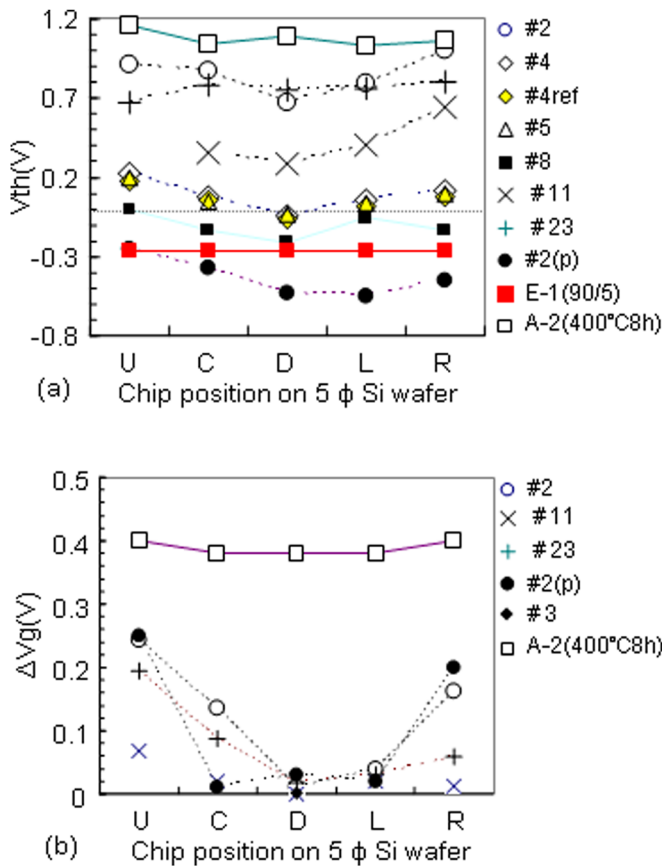


FIG. 4. (Color online) Accumulated device characteristics of as-processed Pt(15 nm)/Ti(5 nm)-gate Si-MOSFETs with different three doses of Table II, as-processed Pt(90 nm)/Ti(5 nm)-gate Si-MOSFETs, hydrogen post-annealed #A-2 chips after air-annealing at 400 °C for 8 h, denoted by A-2 (400 °C 8 h): (a) Threshold voltage V_{th} and (b) hydrogen sensing amplitude ΔV_g .

reference FET in the #4 sensor chips. All of the V_{th} distributions for the as processed FETs except #E-1(90/5) show nearly the same shape in common. The accumulated data about V_{th} are in regular order in accordance with three doses. The variations of V_{th} for n-type FETs with the same (B) dose of $1.0 \times 10^{12} \text{ cm}^{-2}$ show a large value about 0.846 V from -0.04 V to 0.806 V among 4 wafers. It is direct evidence that there are large variations of the total dose of initial unintentional oxygen invasion into the Ti layer at the beginning of the PSG deposition.^{1,2,7} The distributions of V_{th} for both sensor and reference FETs about as-processed #4 chips show nearly the same, where the V_{th} of sensor FETs shows a slightly larger value of about 25 mV in common comparing with that of the reference FETs in the same sensor chips. It means that the work functions of gates are nearly the same at least over the local areas of $1 \text{ mm} \times 1 \text{ mm}$ on the Si wafers because the relative distance of both FETs is 1 mm as shown in Fig. 2(a).

On the other hand, the distribution of V_{th} for p-type FETs, #2(p), shows similar distribution in shape for n-type FETs. If the channel doses of P^+ for n-type FETs and BF_2^+ for p-type FETs are assumed to be uniform over the Si wafers, and the work functions of gates are nearly the same for two FETs, the difference of V_{th} between n-type FETs and p-type FETs will approximately be written by

$$V_{th}(n) - V_{th}(p) \approx E_g(\text{Si}), \quad (3)$$

where $V_{th}(n)$ and $V_{th}(p)$ denote the V_{th} for n-type FETs and p-type FETs, and $E_g(\text{Si})$ is the Si bandgap at the operation temperature.⁹ The average $V_{th}(n) - V_{th}(p)$ in the same chip position for #2 samples is 1.281 V with standard deviations of 0.116 V as shown in Fig. 4(a). As the relative distance of gate regions between #2 and #2(p) in the same chip positions is about 2.24 mm, over which areas the same work function cannot be assured, the average value of 1.281 V seems to be a close value, 1.10 eV of $E_g(\text{Si})$ at 115 °C.⁹ These agreements between experiments and theories also support the oxygen invasion models of the as processed Pt(15 nm)/Ti(5 nm)-gate Si-MOSFETs.

The wafer distributions of ΔV_g show strong correlation with that of V_{th} as shown in Figs. 4(a) and 4(b). The higher V_{th} has a tendency to show the larger ΔV_g in general. It is not clear why most of the sensor chips such as #8 showed no responses over the wafer and a few sensor chips such as #2 showed weak hydrogen-responses with characteristic distributions linked to V_{th} distributions.² We have analyzed these points in Sec. III C.

The average V_{th} of the Pt-Ti-O gate Si-MISFETs denoted by “□ A-2(400 °C 8 h)” was 1.076 V with σV_{th} of 52.2 mV. The Pt (90 nm)/Ti(5 nm)-gate Si-MOSFETs denoted by #E-1(90/5) showed an extremely high uniformity of V_{th} , -0.26 V , where σV_{th} showed a small value of 4.5 mV. It means that the thicker Pt layers protect the Ti layer from oxygen invasion from open air. If we assume the proper V_{th} of Ti-gate Si-MOSFETs is realized by the sample #E-1(90/5), the V_{th} for the Ti-gate Si-MOSFETs denoted by $V_{th}(\text{Ti})$, is -0.26 V . It means that the proper V_{th} shift from Pt/Ti-gate MOSFETs without oxygen invasion to the Pt-Ti-O-gate Si-MISFETs should be estimated by the difference between the average V_{th} , 1.076 V, of the Pt-Ti-O gate Si-MISFETs and the $V_{th}(\text{Ti})$, -0.26 V , of the Pt(90 nm)/Ti(5 nm)-gate FETs. The resultant V_{th} shift is estimated to be 1.336 V, which is very close to the difference, 1.32 eV, of vacuum work function between 5.65 eV of Pt and 4.33 eV of Ti. [10] The flat distribution of V_{th} for the as processed Pt(90 nm)/Ti(5 nm)-gate Si-MOSFETs also means that EB evaporation of Pt/Ti does not cause the interface damages of the gate oxide SiO_2 and Si substrates.

On the other hand, it is difficult to determine the V_{th} without influences of oxygen invasions from the analysis of as processed Pt(15 nm)/Ti(5 nm)-gate Si-MOSFETs sensor chips in Fig. 4(a) because Pt thickness is so thin to protect oxygen invasions. In order to investigate the influence of Pt/Ti layer thicknesses and/or the oxygen invasion to device characteristics, we have prepared several sets of Pt/Ti pairs with different thicknesses of Pt and Ti films including the Pt (15 nm)/Ti(5 nm) pair for the gate metals of Si-MOSFETs, as listed in Table I. The Pt/Ti film deposition conditions were not altered, except deposition times. When the Pt and Ti thicknesses were changed from 15 to 90 nm and from 3 to 45 nm, respectively, we have applied the standard air-annealing at 400 °C for two hours to these sensor chips. The difference of V_{th} , $\Delta V_{th}(s-r)$, between the sensor and

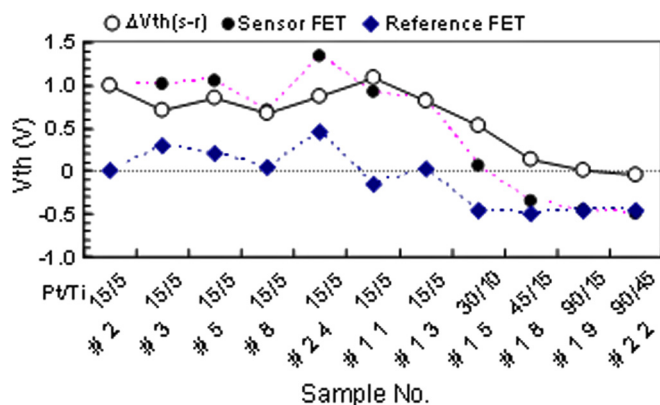


FIG. 5. (Color online) Comparison of V_{th} between sensor and reference FETs with various Pt/Ti thicknesses that are annealed in air at 400°C for two hours. The $\Delta V_{th}(s-r)$ (\circ) represents the V_{th} difference between sensor and reference FETs.

reference FETs in the same sensor chip position U for various Pt/Ti-gate Si-MOSFETs (Table I) after air annealing at 400°C for two hours is summarized in Fig. 5, where the threshold voltages of sensor and reference FETs are also shown. The gate was $10\ \mu\text{m}$ long and $150\ \mu\text{m}$ wide for all the FETs of #11, #13, #15, #18, #19, and #22. The other sensor chips have the standard dimensions of $L_g = 20\ \mu\text{m}$ and $W_g = 300\ \mu\text{m}$. The positively correlated spreads of V_{th} between the sensor and reference FETs on the same sensor chips for the Pt(15 nm)/Ti(5 nm)-gate chips of #2, #3, #5, #8, #24, #11, and #13 with different channel ion doses indicate that the initial unintentional oxygen invasion to both sensor and reference FETs will be the same even if considering wafer to wafer or location to location spreads of the amount of oxygen invasion into the Ti-layers. It also means that the variations of $\Delta V_{th}(s-r)$ will be expected to be small irrespective of channel ion doses or the large variations of initial unintentional oxygen invasion. The average $\Delta V_{th}(s-r)$ for the Pt(15 nm)/Ti(5 nm)-gate chips of #2, #3, #5, #8, #24, #11, and #13 was $0.8579\ \text{V}$ with $\sigma\Delta V_{th}$ of $148.5\ \text{mV}$. Furthermore, $\Delta V_{th}(s-r)$ decreased to about $0\ \text{V}$ by increasing the Pt thickness from 30 to 90 nm. This behavior of $\Delta V_{th}(s-r)$ means that the thicker Pt layers prevent oxygen invasion into the Ti layers from open air during the course of air-annealing process. In this case the V_{th} of both sensor and reference FETs will be determined by the work function of Ti instead of Pt due to the less influenced Ti contacts to the gate insulator of SiO_2 . The average V_{th} of reference FETs for #15, #18, #19, and #22 was $-0.47\ \text{V}$ with $\sigma\Delta V_{th}$ of $20.0\ \text{mV}$. It means that the proper V_{th} shift from the Pt(15 nm)/Ti(5 nm)-gate sensor FETs without oxygen invasion to the Pt-Ti-O-gate Si-MISFETs should be estimated by the difference between the above average $\Delta V_{th}(s-r)$ of $0.8579\ \text{V}$ and the average V_{th} , $-0.47\ \text{V}$, of reference FETs for #15, #18, #19, and #22. The resultant V_{th} shift is estimated to be $1.3279\ \text{V}$, which is very close to the difference, $1.32\ \text{eV}$, of vacuum work function between $5.65\ \text{eV}$ of Pt and $4.33\ \text{eV}$ of Ti.¹⁰

The above two approaches from Fig. 4(a) and Fig. 5 indicate that the V_{th} change before and after annealing procedures can be well explained by a simple device model

based on the difference of work functions of gate metals between $5.65\ \text{eV}$ of Pt and $4.33\ \text{eV}$ of Ti.

The above threshold voltages for Ti-gate Si-MOSFETs denoted by $V_{th}(\text{Ti})$ show two different values of $-0.26\ \text{V}$ by the sample #E-1(90/5) and $-0.47\ \text{V}$ by the reference FETs for #15, #18, #19, and #22. The difference of $V_{th}(\text{Ti})$, $0.21\ \text{V}$, will probably be derived from the reproducibility channel ion doses among different lots of #H18 and #H19 in Table I.

C. Control mechanism of V_{th} for Pt-Ti-O gate Si-MISFETs

The strong correlation between V_{th} and ΔV_g in Fig. 4 suggests phenomenologically that the higher V_{th} has a tendency to show the larger ΔV_g under the same channel ion dose conditions. The spacing of the I-V curves between #5U and #8U, $0.181\ \text{V}$, is close to the theoretical spacing of $0.167\ \text{V}$ expected from Eq. (2). However, the spacing of the I-V curves between #2U and #5U, $0.740\ \text{V}$, is far from the theoretical spacing of $0.167\ \text{V}$. Two samples of #5U and #8U show no hydrogen response and the sample #2U shows hydrogen response as shown in Fig. 4(a). These results suggest the theoretical spacing of $0.167\ \text{V}$ should be realized without any oxygen invasion into the Ti layer until near the gate oxide SiO_2 .

All data of threshold voltages for the n-type as-processed FETs except #4ref and #E-1 in Fig. 4(a) are tuned to the V_{th} for (B) dose of $1.0 \times 10^{12}\ \text{cm}^{-2}$, that is, the V_{th} is replaced by $V_{th}-0.167\ \text{V}$ for (A) dose of $0.8 \times 10^{12}\ \text{cm}^{-2}$ and replaced by $V_{th}+0.167\ \text{V}$ for (C) dose of $1.2 \times 10^{12}\ \text{cm}^{-2}$. These threshold voltages are denoted by $V_{th\text{eff}}$.

All data of ΔV_g for the as processed Pt(15 nm)/Ti(5 nm)-gate Si-MOSFETs except #4ref in Fig. 4(b) are plotted by black circles (\bullet) in Fig. 6. The data of ΔV_g for the Pt-Ti-O-gate Si-MISFETs sensor chips are plotted by circles (\circ) in Fig. 6, which are derived from # A-2 (400°C 8 h) in Fig. 4(b), and also derived from the sensor chips of #2, #3, #8, #23, and #24 chips; the basic sensing characteristics of Eq. (1) are obtained by these five sensor FETs with

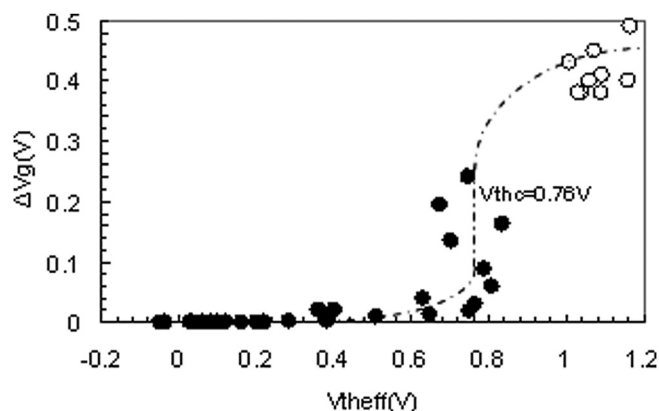


FIG. 6. The sensing amplitude of ΔV_g for accumulated as-processed Pt(15 nm)/Ti(5 nm)-gate Si-MOSFETs in Fig. 4(a) and hydrogen post-annealed Pt-Ti-O gate Si-MISFETs as a function of $V_{th\text{eff}}$ tuned to the dose of (B) $1.0 \times 10^{12}\ \text{cm}^{-2}$. The definition of $V_{th\text{eff}}$ is derived from V_{th} as follows: The V_{th} is replaced by $V_{th}-0.167\ \text{V}$ for (A) dose of $0.8 \times 10^{12}\ \text{cm}^{-2}$ and replaced by $V_{th}+0.167\ \text{V}$ for (C) dose of $1.2 \times 10^{12}\ \text{cm}^{-2}$, and the V_{th} is not changed for (B) dose of $1.0 \times 10^{12}\ \text{cm}^{-2}$.

$L_g = 10 \mu\text{m}$ and $W_g = 150 \mu\text{m}$.² In case of the Pt-Ti-O-gate Si-MISFETs with $L_g = 10 \mu\text{m}$ and $W_g = 150 \mu\text{m}$ the V_{th} was about 89 mV less value in average than that of the standard FETs with $L_g = 20 \mu\text{m}$ and $W_g = 300 \mu\text{m}$ under the same ion implantation conditions. We have corrected V_{th} in $V_{th\text{eff}}$ by 89 mV in the case of circles (○) in Fig. 6.

Figure 6 shows that the sensing amplitude ΔV_g rises up sharply around 0.76 V of $V_{th\text{eff}}$ (V), which is cited as V_{thc} . The value of V_{thc} is 0.316 V smaller than the average V_{th} , 1.076 V, of the Pt-Ti-O gate Si-MISFETs. When regarding the V_{th} of the Ti-gate Si-MOSFETs with (B) dose condition as $V_{th}(\text{Ti})$ discussed in Sec. III B, the difference of $V_{thc} - V_{th}(\text{Ti})$, $1.02(=0.76 - (-0.26))$, is 0.3 V smaller than the difference, 1.32 eV, of vacuum work function between 5.65 eV of Pt and 4.33 eV of Ti.

The physical meaning of V_{thc} can be probably described by a following scenario of the V_{th} change due to oxygen invasion into Ti layers as shown in Fig. 7. When Ti layers contact with gate oxide SiO_2 uninfluenced by the oxygen invasion, uniform Ti contact will be realized over the gate oxides. Some parts of Ti layers, probably under the Pt grain boundaries, will be changed locally to the novel mixing layers of nanocrystalline TiO_x and superheavily oxygen-doped amorphous Ti by the unintentional oxygen invasion at the beginning of PSG deposition. Figure 7(a) represents schematically this situation by a planar view of the surface of gate oxide SiO_2 contacted with gate metals; the dashed short lines represent the Pt grain-boundary triple junctions and the loops represent initial Ti novel mixing layers contacted with gate oxide SiO_2 . In this case the metal contact regions over gate oxide SiO_2 are composed of Ti contact regions and effective Pt contact regions. The Ti novel mixing layers will grow laterally in accordance with increasing oxygen invasion; then the effective Pt contact regions will become dominant. Furthermore, the ratio of Ti contact regions and the effective Pt contact regions will be shrunken up to zero in accordance with increasing the dose of oxygen invasion, which point probably corresponds to the V_{thc} . Figure 7(b) represents schematically this situation around V_{thc} . Finally the Ti novel mixing layers fill up all the Ti layers that correspond to the Pt-Ti-O gate structures as

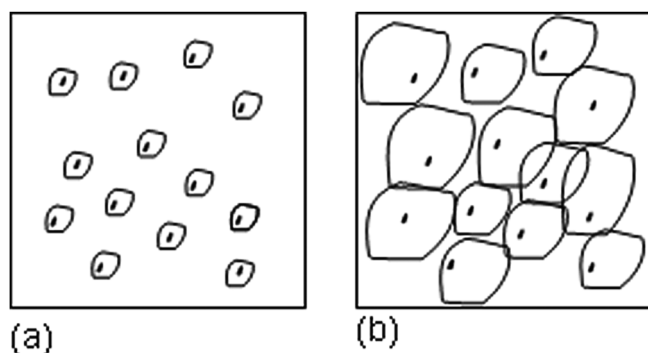


FIG. 7. Schematic planar view of the interface between gate oxide SiO_2 and Ti mixing layers about the proposed percolation model of the gate structures: (a) As processed Pt(15 nm)/Ti(5 nm)-gate Si-MOSFETs and (b) oxygen invasion into Ti layers through Pt grain boundaries. The dashed short lines represent the Pt grain-boundary triple junctions and the loops represent Ti novel mixing layers contacted with both Pt-gate metals and gate oxide SiO_2 .

shown by circles (○) in Fig. 6. In this case the electrical properties of the Ti novel mixing layer will be changed to semiconductor or insulator so that the thin Ti layer should be depleted without free carriers. These depleted Ti layers should make only a minor contribution to the V_{th} .

The uniformity and reproducibility of V_{th} for the hydrogen post-annealed Pt-Ti-O gate Si-MISFETs are shown in Figs. 8(a) and 8(b) among 18 chips of #A-2 including the five chips of #A-3. The average V_{th} and σV_{th} of #A-2 and #A-3 are $V_{th} = 1.081 \text{ V}$ with $\sigma V_{th} = 59 \text{ mV}$ and $V_{th} = 1.0415 \text{ V}$, and $\sigma V_{th} = 39 \text{ mV}$, respectively. The gate was $20 \mu\text{m}$ long and $150 \mu\text{m}$ wide for both FETs. From the practical-application point of view, the hydrogen post-annealing procedure to the Pt-Ti-O gate Si-MISFETs is necessary to terminate the deep traps to reduce the residual sensing amplitude ΔV_{gres} with slow tailing behavior after turning off the hydrogen exposure.² The hydrogen post-annealing procedure also contributes the uniform distribution of V_{th} over wafer, as shown in Fig. 8(b), where the data of σV_{th} for the as-processed chips, the air-annealed chips, and hydrogen post-annealed chips of six different wafers are summarized. The average V_{th} and the standard deviation of the V_{th} , σV_{th} , for as-processed chips and #A-3 among the representative five chip positions (U, C, D, L, R) on the 5- ϕ Si wafer were 0.5427 V and 183 mV, respectively. The larger spread of V_{th} for as-processed chips was originated from the initial unintentional spreads of oxygen invasion.

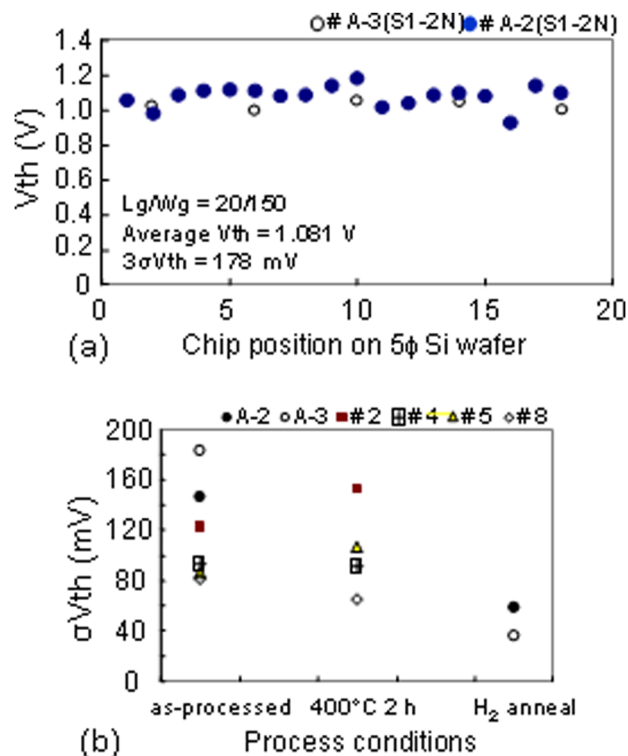


FIG. 8. (Color online) Uniformity and reproducibility of the V_{th} for Pt-Ti-O gate Si-MISFETs hydrogen gas sensors: (a) Wafer distribution and reproducibility of V_{th} for hydrogen post-annealed Pt(15 nm)/Ti(5 nm)-gate Si-MOSFETs for two sensor wafers, #A-2 and #A-3. L_g and W_g are 20 and $150 \mu\text{m}$, respectively. (b) Standard deviations of V_{th} , σV_{th} , for as-processed chips, air-annealed chips, and hydrogen post-annealed chips of six different wafers.

The improvement of uniformity of V_{th} after air annealing will be caused by the sufficient oxygen invasion into the Ti layer, because it will homogenize the initial oxygen distribution in the Ti-layers of as-processed sensor chips. Furthermore, more improvement of uniformity for V_{th} after hydrogen post-annealing will be achieved by the hydrogen compensation to deep traps generated around gate insulators. The uniformity and reproducibility of V_{th} is sufficient for most interface circuit designs.

IV. DISCUSSION AND CONCLUSIONS

The controllability of V_{th} for Pt-Ti-O gate Si-MISFETs hydrogen gas sensors is found to be unexpectedly excellent because of the following reasons. The oxygen invasion process through Pt grain boundaries to Ti layers is not so-called dopant diffusion process to control the carrier density of semiconductors such as Si or GaAs where the mother crystal structures do not change. During the course of oxygen invasion process, at the same time, titanium evacuates to the platinum surface through platinum grain boundaries. The invading oxygen is balanced with the evacuating titanium so that the titanium layer keeps nearly the same thickness as that of the as-grown state. The oxygen-invaded Ti layers change to a kind of new materials; Novel mixing layers of nano-crystalline TiO_x and super-heavily oxygen-doped amorphous Ti formed on SiO_2/Si substrates. The annealing temperature is too low to grow crystalline TiO_x filling up Ti layers. The Ti mixing layers change from metals to semiconductors or insulators. As the Ti layers are so thin like 5 nm, the total amount of oxygen invaded into Ti layers will be saturated and stabilized. From the device operation point of view, it is crucial to control the V_{th} precisely that the Ti novel mixing layers are thin and fully depleted; it is supported by the fact that the V_{th} change before and after air-annealing procedures can be well explained by the difference of vacuum work function between Pt and Ti. Our proposed percolation model to explain the above experimental results should be verified from various characterization methods in future works.

We have found that one of the advantages of the Pt-Ti-O gate Si-MISFETs is uniformity and reproducibility of V_{th} in addition to large sensing amplitudes at the practically important hydrogen concentration range between 100 ppm and 1% and the long intrinsic lifetime of more than 10 years.

ACKNOWLEDGMENTS

This work was supported in part by the New Energy and Industrial Technology Development Organization (NEDO) in Japan. The hydrogen sensor wafers were fabricated in Takasaki Works, Renesas Technology Corp. The authors would like to express sincere thanks to Dr. Yasushi Goto and Dr. Kouichi Yokosawa for their technical support on the fabrication methods of Si-MOSFETs, and Dr. Haruo Takeda, Dr. Hideyuki Matsuoka, Dr. Kazuo Saito, Dr. Hiromasa Takahashi, and Dr. Yumiko Igarashi for their continual encouragements.

APPENDIX: TRIALS FOR BEST AIR-ANNEALING CONDITIONS OF PT(15 nm)/TI(5 nm) GATE SI-MOSFETS

We first selected ten sensor chips in the U regions presented in Fig. 2(b) for each of the three wafers with different doses, #3, #24, and #8. We investigated the annealing temperature dependence of device characteristics at a fixed annealing time of two hours in air. The experimental results of V_{th} and ΔV_g for #3U, #8U, and #24U chips are shown in Fig. 9. Low-temperature annealing less than 300 °C for two hours did not improve ΔV_g , but gradually increased the V_{th} . High-temperature annealing above 450 °C for two hours began to decrease ΔV_g and V_{th} . The FET characteristics and sensing amplitudes of the air-annealed samples at 600 °C for two hours could not be measured due to the destroyed Al wirings.

According to this annealing temperature dependence, the optimum annealing temperature is around 400 °C or 425 °C at air annealing for two hours; therefore, we fixed the annealing temperature at 400 °C, as low as possible, for low-temperature annealing. In fact the resistances of Al wiring heaters begin to degrade the resistance for long heating at 425 °C.⁵

We also prepared ten sensor chips in the C regions of the 5 inch. Si wafers for #8 and #24, and then we measured ΔV_g of two chips, #8 C, and #24 C, for various annealing times t under the fixed annealing temperature of 400 °C, as shown in Fig. 10, where the measurement times for the first five steps were 5, 10, 15, 30, 45 min. The initial value of ΔV_g , i.e., $t=0$ min, shows the ΔV_g of the as-processed chips. The first 15 to 30 min reached saturated ΔV_g , which means the oxidation process of Ti layer was so rapid.

The initial spreads of ΔV_g observed at the as-processed chips in both Fig. 9(b) and Fig. 10 can be interpreted in terms of the initial unintentional spreads of oxygen invasion into the Ti layer, where oxygen invasion should be caused through open air at 390 °C for a couple of minutes before

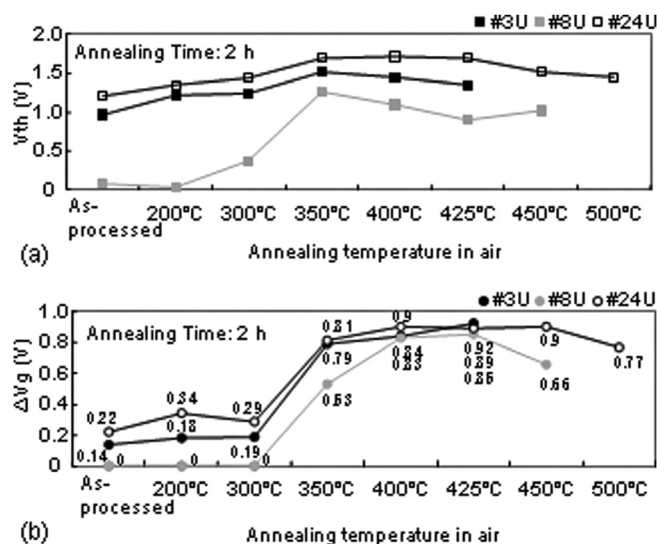


FIG. 9. Annealing temperature dependence of (a) V_{th} and (b) ΔV_g in air at fixed annealing time of 2 h.

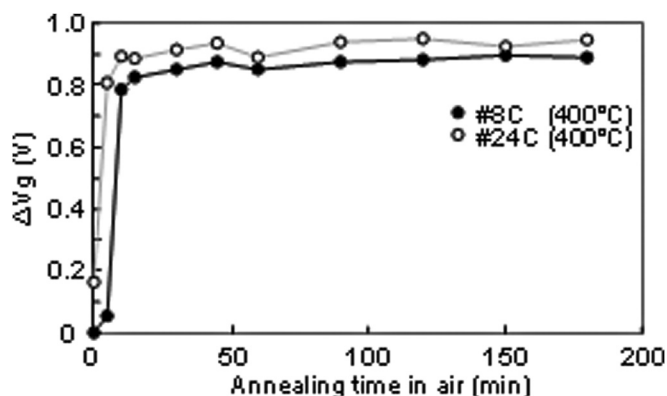


FIG. 10. Annealing time dependence of ΔV_g in air at fixed annealing temperature of 400 °C.

starting thermal chemical deposition (CVD) of PSG as was discussed in the last works.^{1,2} The initial large variations of V_{th} for #3U, #8U, and #24U chips, even if considering

different doses of (A) $0.8 \times 10^{12} \text{ cm}^{-2}$, (B) $1.0 \times 10^{12} \text{ cm}^{-2}$, and (C) $1.2 \times 10^{12} \text{ cm}^{-2}$ for n-type FETs, will be explained by the same initial spreads of oxygen invasion into the Ti layer.

¹T. Usagawa and Y. Kikuchi, *Appl. Phys. Express* **3**, 047201 (2010).

²T. Usagawa and Y. Kikuchi, *J. Appl. Phys.* **108**, 074909 (2010).

³T. Usagawa and Y. Kikuchi, *Proc. IEEE Sensors Conf.* **2010**, 2145 (2010).

⁴T. Yamaguchi, T. Kiwa, K. Tsukada, and K. Yokosawa, *Sens. Actuators A* **136**, 244 (2007).

⁵T. Usagawa, Y. Kikuchi, S. Nakano, and D. Kamoto, *J. Fuel Cell. Technol.* **8**, 88 (2009)[in Japanese].

⁶For examples, J. T. Clemens, *Bell Labs. Tech. J.* **2**, 76 (1997).

⁷T. Usagawa and Y. Kikuchi, Device Analysis of Pt/Ti gate Si-MOSFETs Hydrogen Sensors - Unintentional Oxygen Invasion into the Ti layers, *Jpn. J. Appl. Phys.* (submitted).

⁸J. F. Gibbons, *Proc. IEEE* **56**, 296 (1968).

⁹S. M. Sze, *Physics of Semiconductor Devices*, 2nd ed. (Wiley & Sons, New York, 1981), pp. 442–477.

¹⁰H. B. Michaelson, *J. Appl. Phys.* **48**, 4729 (1977).